Meteorology and Atmospheric Physics (2023) 135:51
https://doi.org/10.1007/s00703-023-00990-1

ORIGINAL PAPER

Future photovoltaic solar power resources in Zambia: a CORDEX-CORE multi-model synthesis

Brigadier Libanda[1] · **Heiko Paeth**[1]

Received: 26 February 2023 / Accepted: 31 August 2023 / Published online: 23 September 2023

Abstract
The exploration of renewable energy such as wind and solar radiation has the potential of reducing reliance on fossil fuels, thus cutting emissions of carbon dioxide, particulate matter, and several other greenhouse gasses. However, recent findings indicate that wind speed across Zambia is very slow, it is increasing but remains unlikely to support large commercial wind farms. In this study, we explore the future impacts of climate change on solar photovoltaic resources. To do this, we examine the new high-resolution (25 km) Coordinated Regional Climate Downscaling Experiment—CORDEX-CORE simulations for the African domain, using two different emission scenarios until 2100. At an annual scale, results indicate a weak but steady decrease in PV_{Res} of around 0.02 W/m^2 per annum under RCP2.6 and about 0.005 W/m^2 per annum under RCP8.5. Results further show that at an average of ~ 237 ± 3.3 W/m^2 and 212 ± 2.5 W/m^2, respectively, RCP2.6 comes along with 12 ± 3% more PV_{Res} than RCP8.5. Thus RCP2.6, a greener and climate-friendly pathway, points towards a higher renewable energy potential across Zambia compared to the business-as-usual pathway.

Keywords Renewable energy · Photovoltaic potential · CORDEX-CORE · Regional climate modelling · Climate change · Zambia

1 Introduction

Over the past decade, the cost of renewable energy has been declining steadily. The weighted average of the levelized cost of electricity at the global level fell by 15% for wind and 13% for solar energy in 2021 alone (Irena 2022). Over the past 5 years, the cost of solar energy has been declining at the rate of 13% per year while it was 7% for onshore wind energy (Lazard 2020). These trends have the potential to incentivize carbon neutrality and contribute to tackling the climate crisis by reducing reliance on fossil fuels (Pfeifer et al. 2021; Luderer et al. 2021).

To date, the burning of fossil fuels remains one of the largest producers of carbon greenhouse gasses contributing ~ 66% of global CO_2 emissions (Foster and Elzing 2015). Evidence suggests that in less than a couple of decades, anthropogenic activities have doubled the atmosphere's CO_2 content since the beginning of industrialization (NASA 2022). The presence of CO_2 in the atmosphere warms the earth and this leads to synoptic-scale changes in the climate system (Herwartz et al. 2021; Hartley and Turnock 2021). Most of these climatic changes which include extreme rainfall events such as floods and droughts impose cascading risks on lives, critical infrastructure, and property. Therefore, a shift to clean energy contributes to achieving Sustainable Development Goals Number 7 and 13 which stress the importance of ensuring access to affordable clean energy through climate action (UN 2015).

While critiques of renewable energy cite the spatiotemporal variability of wind and solar radiation as a weakness to a dependable electricity grid (Diesendorf and Elliston 2018), this shortcoming can be overcome by renewable energy mixes including wind, water, and solar power. Furthermore, technological advancements such as innovative energy storage, and optimized management techniques show promise of turning wind and solar energy resources into dependable electricity grids. Indeed, renewable energy sources like solar and wind energy are constantly being replenished at a higher rate than what humans can consume.

Responsible Editor: Clemens Simmer, Ph.D.

✉ Brigadier Libanda
brigadier.libanda@uni-wuerzburg.de

[1] Institute of Geography and Geology, Physical Geography, University of Wuerzburg, Würzburg, Germany

Many countries in the developed and developing world are turning to renewable energy as a pathway to climate change mitigation. The European Union for instance is accelerating the take-up of renewables to significantly contribute to the reduction of net greenhouse gas emissions by at least ~ 55% before the end of 2030 (EU 2022). In Africa, many countries including but not limited to South Africa, Nigeria, and Kenya have also set strong emissions-reduction targets. Zambia has also committed to reducing emissions by 25% by 2030 (USAID 2015). Overall, Africa has committed to cutting 32% of emissions by 2030 (Abudu et al. 2023).

With these emissions-reduction ambitions, global renewable energy is expected to expand rapidly. Projections show that by 2024, the global capacity of renewable energy will increase by 50%, and 60% of this will be sourced from solar photovoltaic resources (IEA 2019). During the same period, additional 22 gigawatts of renewable energy are expected across sub-Saharan Africa alone (IEA 2019). While these ambitions and projections will have a profound effect on CO_2 emissions, it is notable that climate change, in turn, will also affect the future variability of wind and solar energy resources, affecting the ability of countries to produce electricity using renewables. Therefore, studies that assess future changes in climatic variables are indispensable for future renewable energy systems (Troccoli et al. 2018).

The overarching objective of this study is to explore future variations of climatic variables that are relevant to future photovoltaic solar power resources (PV_{Res}) in Zambia. While much of Zambia experience roughly similar climate characteristics due to the plateau that characterizes the country's topography (Fig. 1A), a few climatic differences exist, and these can be classified into four main categories of the Köppen–Geiger classification (Peel et al. 2007):

1. *Tropical Savanna* The Tropical Savanna climate which is classified as *Aw* in the Köppen–Geiger classification covers Kalabo district, parts of Shang'ombo, and Mongu in the Western Province of Zambia (Fig. 1B). In the Eastern Province, Katete, Petauke, and parts of Chipata are also classified as Tropical Savana. These areas generally experience a pronounced dry season characterized by monthly rainfall averaging 60 mm (Africa Groundwater Atlas 2019).
2. *Arid Steppe* This climate zone covers the semi-arid region of Livingstone, Kaloma, Choma, and parts of the Luangwa valley (Fig. 1B). While the rainfall in these areas is not as low as that of desert climates, it is usually less than potential evapotranspiration and can, thus, be described as semi-arid.
3. *Temperate with dry winters (generally June–August, see* Marshall 2017*) and warm summers* The *Cwb* climate of Zambia mainly covers the northern tip of the country bordering the Democratic Republic of the Congo and Tanzania (Fig. 1B). These areas include Kaputa, Mpulungu, and Mbala. Given their high elevations, temperatures are usually lower than across the rest of the country.

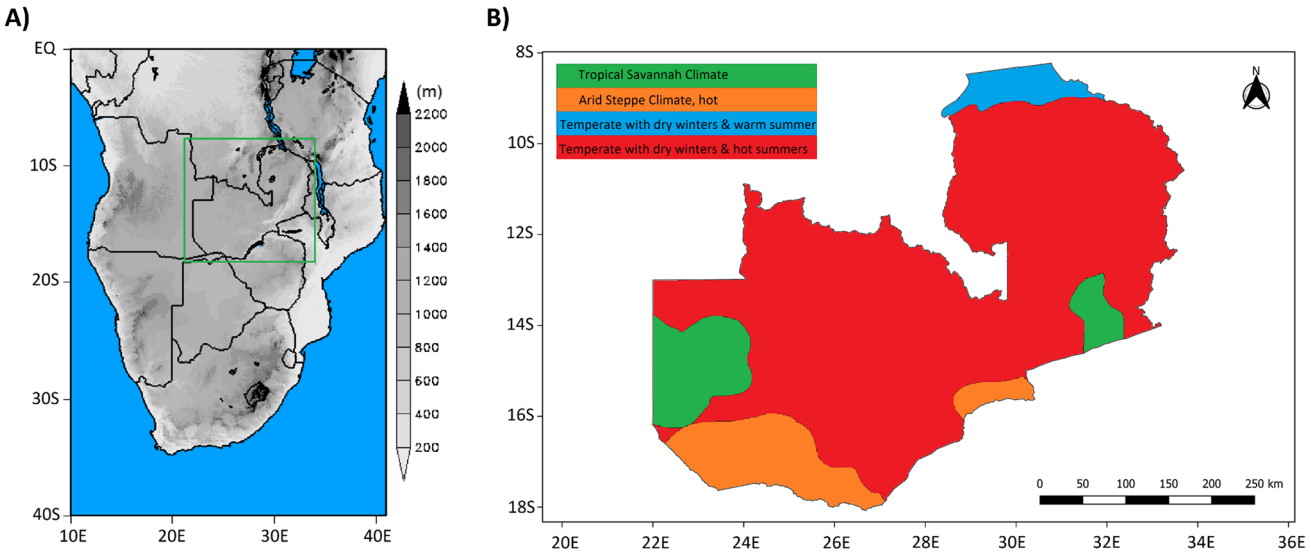

Fig. 1 Overview of the study area showing: **A** the location of Zambia in Southern Africa (green square). The grey shading indicates topographical variations across the region based on the Global Land 1 km Base Elevation (GLOBE) digital elevation model (Hastings and Dunbar, 1999). The blue shading shows the location of major water bodies, **B** climatic zones of Zambia were developed using the Climatic Research Unit Time Series Version 3.21 (CRU TS 3.21) dataset produced and maintained by the Climatic Research Unit of the University of East Anglia (Jones and Harries 2013). The precipitation and temperature CRU data used to produce the Climatic Zones of Zambia are for the period 1951–2010 (Africa Groundwater Atlas 2019)

Table 1 Summary of the reference datasets used in this study. The 1981–2005 period used in this study was chosen to align with the availability of climate model datasets

Variable	Source	Resolution	Period used
Air temperature	Harris et al. (2020)	0.5°	1981–2005
Wind speed	Hersbach et al. (2020)	0.1°	1981–2005
Downwelling surface shortwave solar radiation	Abatzoglou et al. (2018)	4 km	1981–2005

4. *Temperate with dry winters and hot summers* Classified as *Cwa* in the Köppen–Geiger classification (Peel et al. 2007), this climate zone covers the rest of the country which is mainly characterized by dry winters and wet summers.

2 Data and methods

2.1 Data

2.1.1 Reference datasets

To perform the present analyses, we explored three different atmospheric variables which include air temperature measured at 2 m above sea level (TAS), wind speed measured at 10 m above sea level (WS), and downwelling surface shortwave solar radiation (SR).

TAS was sourced from the latest version of high-resolution monthly data (CRU TS v4.05) from the Climatic Research Unit of the University of East Anglia (Harris et al. 2020; Table 1). The dataset covers all land areas across the globe apart from Antarctica and is gridded at a resolution of 0.5°. CRU TS v4.05 was developed using angular-distance weighting to interpolate in situ data from a dense network of meteorological stations across the globe (Harris et al. 2020).

For wind speed, we used the fifth-generation global climate reanalysis (ERA5). ERA5 is a product of the European Centre for Medium-Range Weather Forecasts (ECMWF) and was developed by assimilating in situ data into a global weather forecast model (Hersbach et al. 2020). ERA5 has a $0.1° \times 0.1°$ horizontal resolution.

We retrieved SR from the archives of TerraClimate. This is also a high-resolution dataset gridded at 4 km (Abatzoglou et al. 2018). TerraClimate was developed by merging climatological normals from WorldClim version 1.4 and version 2 datasets (Fick and Hijmans 2017), CRU TS v4.0 (Harris et al. 2020), and JRA-55 (Ebita et al. 2011).

2.1.2 Climate models

In this study, we analyzed CORDEX-CORE models. Unlike ordinary CORDEX models, the CORDEX-CORE initiative is an improvement in terms of the horizontal resolution and a general homogenization of simulations across different CORDEX domains (Gutowski et al. 2016). CORDEX-CORE Regional Climate Models (RCMs) can, therefore, be thought of as a homogeneous set of high-resolution projections across all CORDEX domains driven by a common set of General Circulation Models (GCMs).

The CORDEX-CORE models used in the present study are for the historical period 1981–2005 and the future period 2025–2100. The models used include the Germany Climate Service Centre's REMO model (Jacob and Podzun 1997), the Consortium for Small-Scale Modeling (COSMO) community's CCLM (Rockel et al. 2008), and the Abdus Salam International Center for Theoretical Physics' RegCM4 (Giorgi et al. 2012). The horizontal resolution of the CORDEX-CORE models is $0.22° \times 0.22°$. Despite the significant improvements the CORDEX-CORE initiative introduces, our literature review shows that no published peer-reviewed studies exist evaluating photovoltaic solar power resources (PV_{Res}) across Zambia. As such, PV_{Res} across Zambia remain largely unstudied, leading to major uncertainties and

Table 2 Parameterizations of the CORDEX-CORE models used in this study

Model	Institution	Microphysics	Cumulus CONVECTION	Planetary boundary layer	Radiation scheme	Aerosols
REMO	GERICS	Lohmann and Roeckner (1996)	Nordeng (1994)	Louis (1979)	Morcrette et al. (1986)	No aerosol module
CCLM	COSMO and DWD	Doms et al. (2007)	Tiedtke (1989)	Herzog et al. (2002)	Ritter and Geleyn (1992)	No aerosol module
RegCM	ITCP	Pal et al. (2000)	Tiedtke (1989)	Holtslag et al. (1990)	Kiehl et al. (1996)	Organic and black carbon, SO_4, dust, sea salt (Solmon et al. 2006; Zakey et al. 2006; 2008)

REMO, Regional Model; GERICS, The Germany Climate Service Center; COSMO, the Consortium for Small-Scale Modeling; DWD, The Deutscher Wetterdienst i.e., German Meteorological Service; RegCM, Regional Climate Model; ITCP, International Centre for Theoretical Physics

a lack of understanding of how climate change will affect renewable energy potential in the future.

It is important to note that CORDEX-CORE RCMs are only available for two Representative Concentration Pathways (RCPs), i.e., the low-end RCP2.6 and the high-end RCP8.5 scenario (Giorgi et al. 2022). RCP 2.6 is an ambitious target of keeping global temperature increments below 2 °C by the close of the twenty-first century (IPCC 2014). To achieve the RCP2.6 target, emissions should decline and reach zero by 2100. On the other hand, the RCP8.5 is a business-as-usual scenario; emissions continue to rise and as such, it is considered a worst-case scenario (Meinshausen et al. 2011). In this study, we examined both scenarios over the period 2025–2100 (Table 2). We retrieved all simulations from the Earth System Grid Federation (ESGF) node of the German Climate Computing Centre (DKRZ).

2.2 Methods

2.2.1 Conceptual framework and reliability metrics

To establish a reliable understanding of future PV_{Res}, the RCMs used must realistically reproduce the observed historical climate. Therefore, the analysis starts by evaluating the ability of CORDEX-CORE models to simulate TAS, SR, and WS as they are key to the generation of PV_{Res} and, thus, to the renewable energy sector as a whole. Based on data availability, we used the 1981–2005 reference period that is available for the observational and model datasets. This reference period is widely used in renewable energy studies (Costoya et al. 2021; Ogunjobi et al. 2022). To ease the evaluations, we used Climate Data Operators (CDO) to regrid all datasets to a common resolution of the CRU TS v4.05 reference data.

Several methods of model evaluation exist; some are simple and straightforward while others are more complex. For example, some previous studies used percent overlap (PO), arguing that its simplicity in using probability density functions (PDFs) as a statistical measure of how well models reproduce observed PDFs of variables of interest makes it a useful tool (Perkins et al. 2007). In the present study, however, we focus on the ability of models to simulate spatiotemporal patterns as this is of importance when deciding where to install solar farms. In addition, it helps understand the seasonal cycle of solar energy potential with maximum/minimum PV_{Res} to be expected. Using this performance criterion, we were able to exclude simulations whose outputs seemed unrealistic, e.g., those that produce output that is abnormal and in disagreement with the current understanding of the climate of Zambia. Spatiotemporal dynamics of climatic variables are widely used as a performance criterion for models (Cattiaux et al. 2013; Bartók et al. 2019; Vautard et al. 2019).

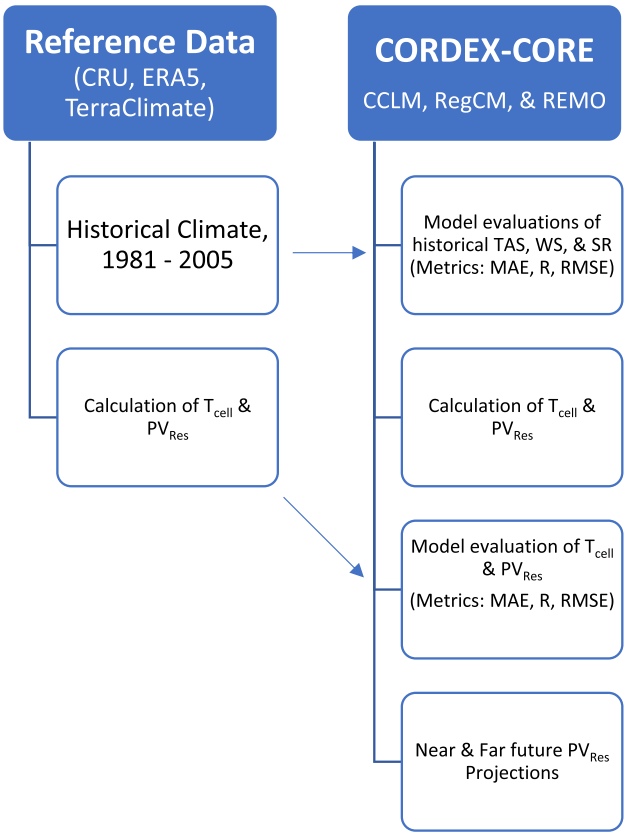

Fig. 2 Conceptual framework followed in the present study. CRU, Climate Research Unit; ERA5, European Centre for Medium-Range Weather Forecasts Reanalysis version 5. REMO, Regional Model; GERICS, The Germany Climate Service Center; COSMO, the Consortium for Small-Scale Modeling; RegCM, Regional Climate Model; TAS, ambient temperature; WS, wind speed; SR, downwelling surface shortwave radiation; T_{cell}, cell temperature; PV_{Res}, solar photovoltaic energy resources, far future: 2025–2055; near future: 2075–2100

To compute the reliability metrics, we used the Satellite Application Facility on Climate Monitoring (CM SAF; Kothe 2022). CM SAF is a toolbox that automates the calculation of several model evaluation metrics in R Programming Language (R Core Team 2020). Some of these metrics include correlation (*R*), root mean square error (RMSE), and mean absolute error (MAE). A summary of the process we followed is given in Fig. 2.

2.2.2 Calculation of solar photovoltaic energy resources

The energy received from the sun touches the earth's surface as shortwave solar radiation and is part of the electromagnetic radiation spectrum (Blal et al. 2020; Spiridonov and Ćurić, 2021). Solar radiation consists of visible light, infrared, ultraviolet light, X-rays, gamma rays, and radio waves. Ultraviolet and visible light together form shortwave downward radiation. It is the only one that has enough energy

density to produce electricity when it reaches a solar cell (Costoya et al. 2022). To calculate solar photovoltaic energy resources (PV_{Res}) in this study, we considered the amount of shortwave downward radiation at the surface and corrected it based on the efficiency of PV cells which generally reduces with increasing temperature (Radziemska 2003). Our calculation of PV_{Res} was based on the work of Jerez et al. (2015) who studied the impact of climate change on PV_{Res}. Mathematically, PV_{Res} can be expressed as follows:

$$PV_{Res} = P_R * RSDS, \tag{1}$$

where RSDS is the shortwave downward radiation at the surface given in W/m^2 and P_R is a performance ratio that considers the effect exerted by temperature on the efficiency of PV cells (Jerez et al. 2015). PR can be expressed mathematically as follows:

$$P_R = 1 + \gamma(T_{cell} - T_{STC}). \tag{2}$$

Here, γ refers to the power thermal coefficient for monocrystalline silicon cells which indicates how strongly the PV power output is dependent on the temperature of the cells. Here, we use a constant value of − 0.005 °C (Tonui and Tripanagnostopoulos 2008). It is negative because the power output is inversely proportional to increasing cell temperature. T_{SRC} refers to the temperature of the cell under standard test conditions and has a constant value of 25 °C. T_{cell} refers to a multiple regression model which considers the effects of solar radiation, temperature, and wind speed (Chennai et al. 2007). It can be expressed as shown in Eq. 3:

$$T_{cell} = c_1 + c_2 * Tas + c_3 * RSDS + c_4 * WS, \tag{3}$$

where Tas is the air temperature around the cells and is given in °C. RSDS is the downward solar radiation at the surface (W/m^2), and *WS* is the near-surface wind speed (m s^{-1}). C_1, C_2, C_3, and C_4 are coefficients that are dependent on the properties of the PV materials used. According to Jerez et al. (2015), we apply the following values:

$C_1 = 4.3$ °C,
$C_2 = 0.943$,
$C_3 = 0.028$ °C m^2 W^{-1}
$C_4 = -1.528$ °C s m^{-1}

2.2.3 PV_{Res} trend analysis

While there are several trend detection methods existing (e.g.,Adamowski et al. 2009; Sonali and Nagesh Kumar 2013), the non-parametric Mann–Kendall trend test (MK test) and its modified version are inarguably the most used in climate research (Tesche and Kumar 2016; Agbo et al. 2022). The modified MK test is especially preferred because it ensures that the time-series data under study are not serially correlated and this prevents the detection of false trends (Hammed and Rao 1998).

In the present study, we employed the modified MK test to quantify the evolution of PV_{Res} trends. To do this, we used the 'modifiedmk' Package (Patakamuri and O'Brien 2021) in R Programming Language (R Core Team 2020). In modified MK tests, the equivalent normal variants of the rank of the de-trended series are obtained using Eq. 5:

$$Z_i = \varphi^{-1}\left(\frac{R_1}{n+1}\right) \text{for} \quad i = 1 : n, \tag{5}$$

where R_i refers to the rank of the de-trended time series, n refers to the length of the time series, and φ^{-1} is the inverse standard normal distribution function with a mean of 0 and a standard deviation of 1 (Hammed and Rao 1998).

2.2.4 Bias correction techniques

In an effort to increase confidence in future PV_{Res} projections, we applied linear scaling (LS) to simulations. LS is a widely used bias-correction technique that considers the difference between mean reference data and model outputs and then applies it to simulations (Ines and Hansen 2006; Shrestha et al. 2015).

3 Results and discussion

3.1 Regional climate model evaluation

During the 1981–2005 reference period, the Regional Climate Models REMO, CCLM, and their ensemble mean reproduce wind speed, TAS, and SR with spatial correlations ranging between 0.5 and 0.7 (Fig. 3 and Table 3). At ~ 2.3 ms^{-1}, the RMSE for wind speed is in the order of the mean wind speed suggesting a generally poor performance across the models. A temperature bias of ~ 3 °C and SR bias of ~ 22 W/m^2 further adds credence to the observation made with wind speed, i.e., the state-of-the-art models exhibit substantial deficiencies in reproducing the observed climate of Zambia. These observations point to the need for a thorough bias correction before analyzing any future trends.

Table 3 Summary of the correlation coefficients between mean annual observed and modeled near-surface wind speed at 10 m (ms^{-1}), downwelling surface shortwave radiation (SR, W/m^2), and near-surface air temperature at 2 m (TAS, °C) during the 1981–2005 period

	CCLM	REMO	Ensemble mean
Wind speed	0.7	0.5	0.5
SR	0.6	0.7	0.8
TAS	0.6	0.7	0.68

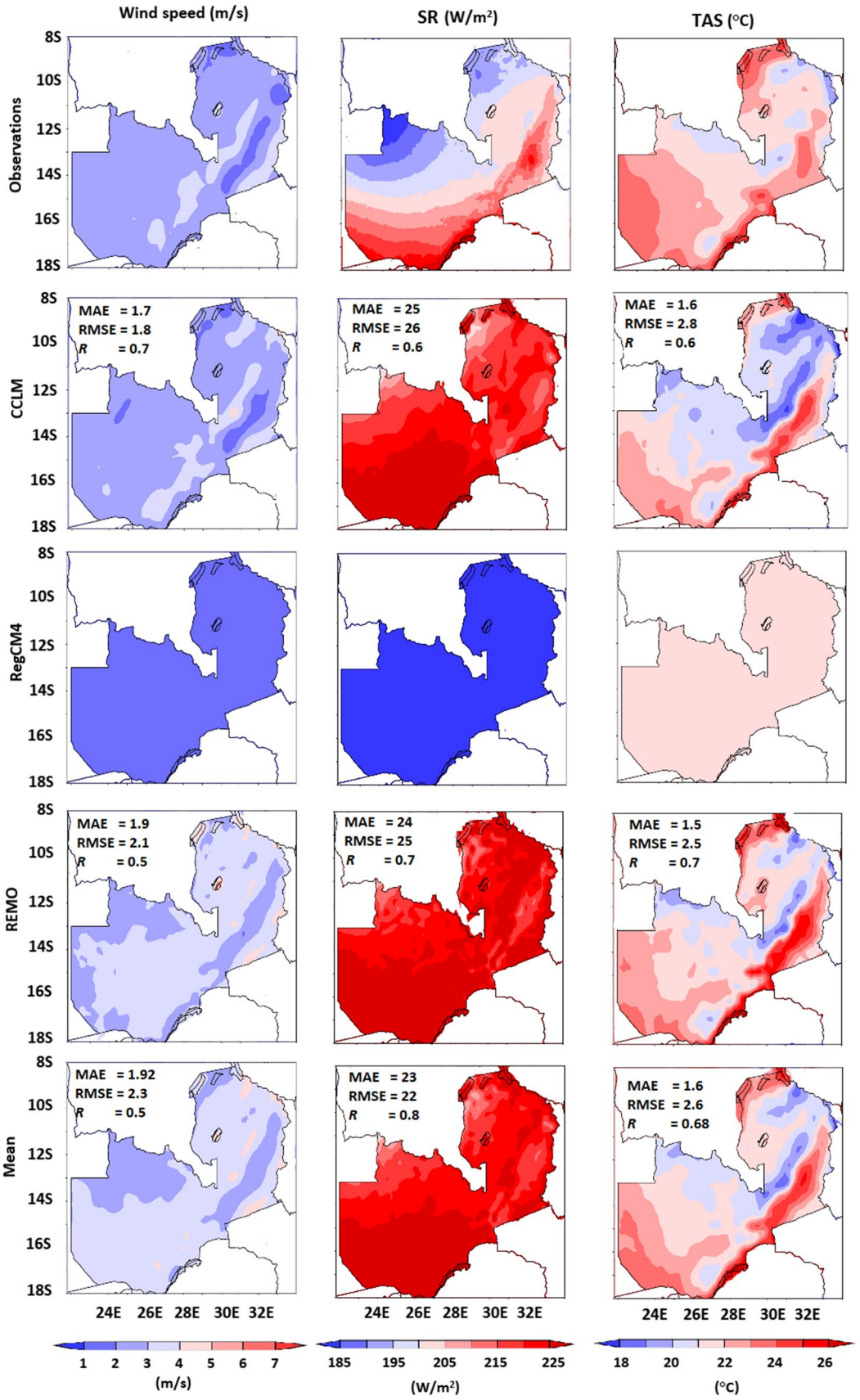
Wind speed (m/s)
SR (W/m²)
TAS (°C)
Observations
CCLM
RegCM4
REMO
Mean
MAE = 1.7
RMSE = 1.8
R = 0.7
MAE = 25
RMSE = 26
R = 0.6
MAE = 1.6
RMSE = 2.8
R = 0.6
MAE = 1.9
RMSE = 2.1
R = 0.5
MAE = 24
RMSE = 25
R = 0.7
MAE = 1.5
RMSE = 2.5
R = 0.7
MAE = 1.92
RMSE = 2.3
R = 0.5
MAE = 23
RMSE = 22
R = 0.8
MAE = 1.6
RMSE = 2.6
R = 0.68
8S
10S
12S
14S
16S
18S
24E 26E 28E 30E 32E
1 2 3 4 5 6 7
(m/s)
185 195 205 215 225
(W/m²)
18 20 22 24 26
(°C)

◂**Fig. 3** Spatial patterns of mean annual observed and modeled near-surface wind speed at 10 m (ms^{-1}; first column), downwelling surface shortwave radiation (W/m^2; middle column), and near-surface air temperature at 2 m (°C; right column) during the 1981–2005 period

Notwithstanding the observed deficiencies, REMO, CCLM, and their ensemble mean show above-average performance, especially considering that they can capture the spatial distribution of the reference dataset with generally higher wind speeds of up to 4 m s^{-1} across the central parts of Zambia while the rest of the country experiences ~ 3 m s^{-1}. Further, the two models and their mean show a downward gradient of SR increasing from the north of the country to the south. While these spatial distributions are captured correctly by the models, it is noticeable that they tend to overestimate SR. Overall, the reference dataset shows SR values of up to 195 W/m^2 around Luapula Province and over the Mwinilunga area of Northwestern Province, but the models and their mean simulate values of ~ 205 W/m^2 (Fig. 3). Regarding TAS, models accurately simulate higher values of 26 °C over the Eastern and Southern Provinces of the country similar to the observational dataset (Fig. 3).

While it is noted in this study that all models struggle with reproducing historical climate, REMO and CCLM perform far better than RegCM. For instance, for TAS and SR, *R* values for REMO are up to 0.7 (TAS, RMSE and MAE are 1.5 °C and 2.5 °C, respectively; SR, RMSE, and MAE = 25 W/m^2 and 24 W/m^2, respectively), and up to 0.5 for WS. For CCLM, *R* values for TAS and SR go up to 0.6 (TAS, RMSE and MAE are 2.6 °C and 1.6 °C, respectively; SR, RMSE and MAE = 25 W/m^2 and 24 W/m^2 respectively). The above-average performance of the two models (i.e., REMO and CCLM) has been documented by other studies such as Ndiaye et al. (2022) who studied future changes in solar PV and wind energy potential over West Africa and found that REMO and CCLM behaved very well across the Guinean coast, Sudan, and Sahelian climatic zones. It is notable, however, that while RegCM performs well across other regions, challenges to simulate wind speed, SR, and TAS are very vivid across Zambia (Fig. 3). The RegCM model notices no climatic variations across the whole country for all three variables. This observation was also made earlier with wind speed simulations (Libanda and Paeth 2022) and may be related to model parameterization, local climate features which RCMs cannot reproduce due to discrepancies in resolution, or observational errors (Wilcke et al. 2013). Given these unrealistic simulations by RegCM, we excluded it from further analyses.

The remaining two RCMs were found to reproduce the observed annual cycle of wind speed, SR, and TAS differently (Fig. 4). The annual cycle of TAS is well captured by the RCMs with the highest values of about 25 °C from October to November and plummeting to ~ 18 °C in June/

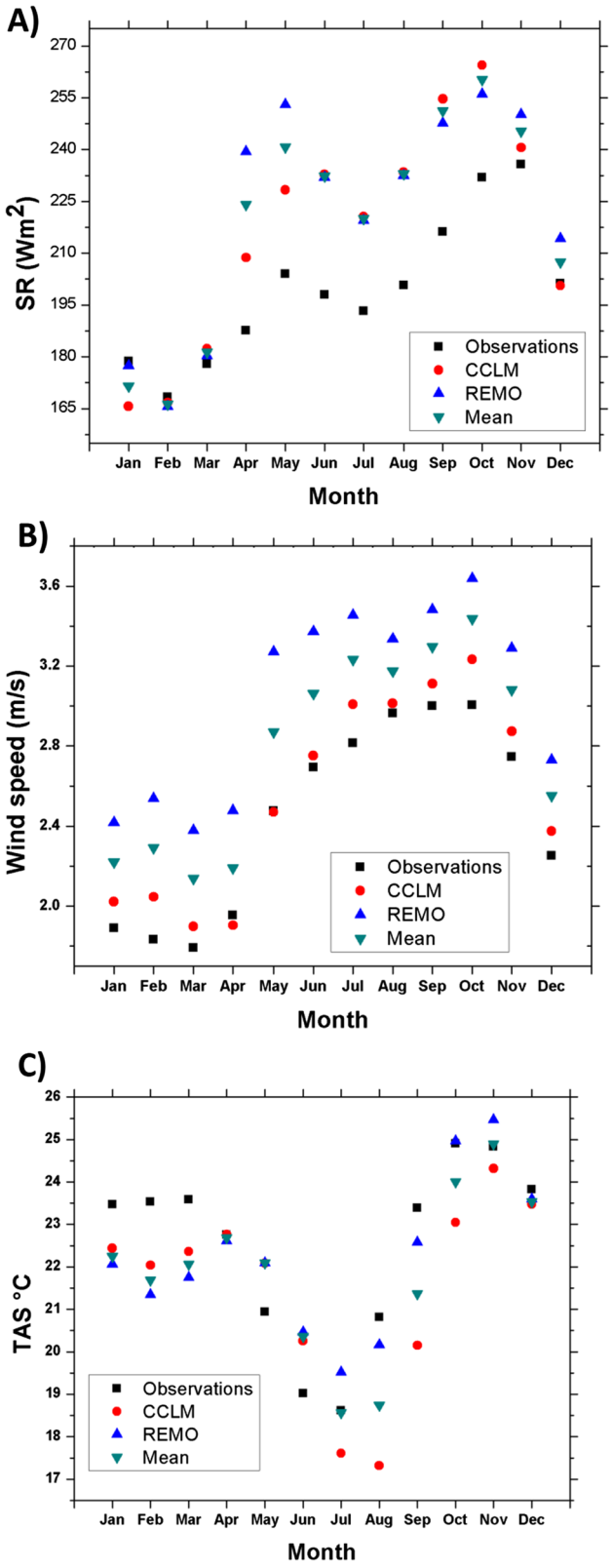

Fig. 4 Mean annual cycle of observed and modeled **a** downwelling surface shortwave radiation (W/m^2), **b** near-surface wind speed at 10 m (ms^{-1}), and **c** near-surface air temperature at 2 m (°C) during the 1981–2005 period, averaged across longitude 21°–34° E and latitude 17.4°–7.6° S

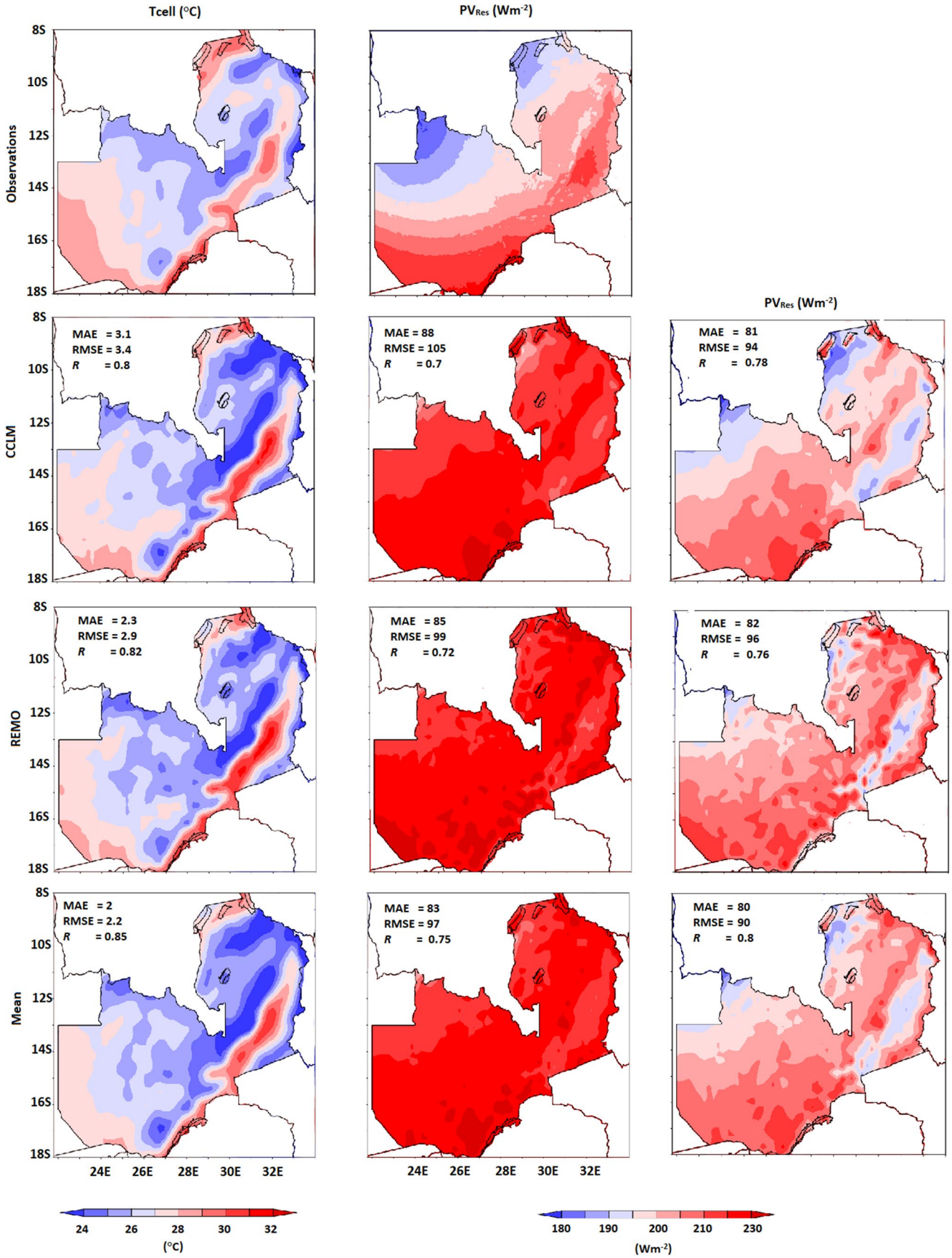
Tcell (°C)
PVRes (Wm-2)
Observations
CCLM
REMO
Mean
8S
10S
12S
14S
16S
18S
24E
26E
28E
30E
32E
MAE = 3.1
RMSE = 3.4
R = 0.8
MAE = 88
RMSE = 105
R = 0.7
PVRes (Wm-2)
MAE = 81
RMSE = 94
R = 0.78
MAE = 2.3
RMSE = 2.9
R = 0.82
MAE = 85
RMSE = 99
R = 0.72
MAE = 82
RMSE = 96
R = 0.76
MAE = 2
RMSE = 2.2
R = 0.85
MAE = 83
RMSE = 97
R = 0.75
MAE = 80
RMSE = 90
R = 0.8
24
26
28
30
32
(°C)
180
190
200
210
230
(Wm-2)

◂**Fig. 5** Same as Fig. 2, but for cell temperature (°C; T_{cell} i.e., column 1), photovoltaic solar power resource (PV_{Res}; W/m^2, column 2), and bias-corrected photovoltaic solar power resource (PV_{Res}; W/m^2, column 3)

July (Fig. 3C). Both RCMs tend to overestimate SR and wind speed (Fig. 4A, B). With an average of 3 ms^{-1}, REMO consistently exhibited a positive bias of 20% compared to the reference dataset. CCLM, on the other hand, shows very good performance with a positive bias of only 4%. At an average of 2.7 ms^{-1}, the mean of the models was 12% higher than the reference dataset. Positive biases are again seen with SR; for instance, REMO was found to exhibit a positive bias of ~ 11% while CCLM again exhibits better performance with a bias of only ~ 8%. The mean of the two models (i.e., REMO and CCLM) was found to be 10% higher than the reference dataset. Overall, both the models and the reference dataset exhibit the lowest SR values around July which constitutes the coldest month in Zambia. The low SR values in July can, therefore, be attributed to the fact that the sun's rays are generally more slanted during July than in other months (Marshall 2017). Regarding TAS, exceptional performance was found with REMO showing a near-zero bias of − 1% while CCLM was found to have − 4% bias. Taken together, the multi-model ensemble exhibited a bias of only − 2% (Fig. 4).

Taken together, the biases found in this work are very minor compared to those found in West Africa where, e.g., wind speed overestimations were as high as 50% (Ndiaye et al. 2022). While interrogating the causes of biases observed herein was beyond the scope of the present study, it is well established that model biases can be caused by a range of factors which may include limited spatial resolution, hence failure to read microscale meteorological processes, simplified thermodynamic processes, and utter incomplete understanding of the physics of the global climate system (ECMWF 2022).

Given the considerable overestimation of solar radiation during austral winter, a systematic overestimation of wind speed especially by REMO, and some minor errors in the seasonal temperature cycle, we calculated cell temperature (T_{cell}) and PV_{Res} during the reference period (1981–2005) and compared the performance of models to the reference data. At first sight, the ability of models to accurately reproduce present-day climate would give credence to their ability to project future PV_{Res}. We found strong and statistically significant correlations of up to 0.8 for T_{cell} (Fig. 5). Similar to the reference dataset, both models and the mean show the highest T_{cell} values of ~ 30 °C along the Luangwa Valley. Regarding PV_{Res}, we noticed that all models simulate the spatial pattern correctly with the highest values over Livingstone and much of the Southern Province. However, some large biases are also noticeable, especially over the Copperbelt where the reference dataset shows PV_{Res} of 190 W/m^2 while models overestimate it at ~ 210 W/m^2. This, therefore, suggests that models can accurately depict areas that are expected to have higher future PV_{Res} although a noticeable systematic overestimation of up to ~ 10 ± 2% should be expected. After applying bias correction, substantial improvements of R values reaching 0.8 are observed (Fig. 5 Column 3). This finding re-echoes the earlier observation that a thorough bias correction prior to analyzing any future trends would be required.

The seasonal evolution of T_{cell} shows that all the models accurately depict month–month changes with all variations correctly mimicked although differences in the mean are evident (Fig. 6). Notably, models underestimate T_{cell} in January and February which represents the core of the rainy season in Zambia (Musonda et al. 2020); this underestimation could be related to models struggling to reproduce cloud cover and precipitation during the rainy season. It is estimated that during the January/February period, close to 70% of the country is characterized by cloudy to overcast conditions punctuated by rapid intermittent periods of sunshine (Nkolola et al. 2021). These cloudy conditions dictate energy budgets with ripple effects on the variability of other climatic variables, especially the amount of solar radiation reaching the earth's surface.

The ability of models to simulate PV_{Res} is lower than that of T_{cell} (Fig. 7). We found a good representation in terms of the basic structure of the annual cycle but a substantial overestimation from March to November. Notwithstanding these biases, the lower bounds during the rainy season in January and February are simulated correctly: PV_{Res} based on the reference dataset ranges from 165 to 229 W/m^2 while that of CCLM, REMO, and the mean are 163–259 W/m^2, 164–250 W/m^2, and 165–255 W/m^2, respectively (Fig. 7). These results suggest that future projection based on these models will give reliable ranges for minimum solar radiation whereas the maximum is fairly overestimated.

Substantial biases of the maximum values of solar radiation reported herein were also found in West Africa where CORDEX-CORE models were used to study photovoltaic potential (PVP; Ndiaye et al. 2022). However, while RCMs overestimate PV_{Res} in Zambia from March to November, they were found to underestimate it in West Africa, pointing to a regionally inhomogeneous bias in cloudiness across Africa. To get a reliable estimate of PV_{Res} projections, we applied a delta change bias correction to the mean and found a 9.2% improvement (Fig. 7).

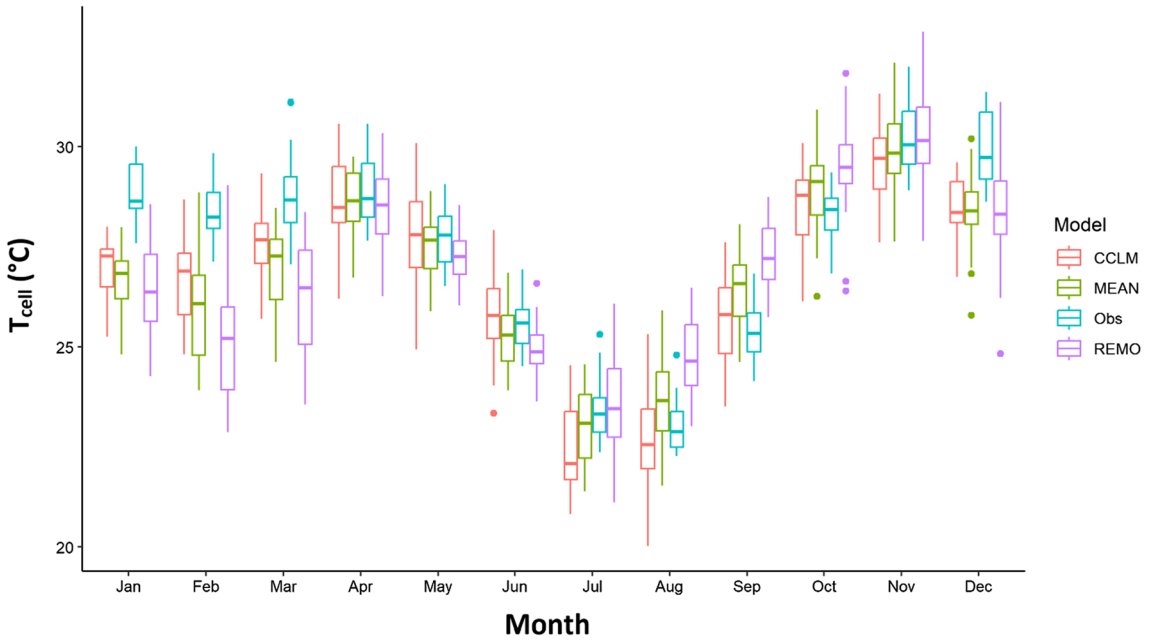

Fig. 6 Mean annual cycle of observed and modeled T_{cell} (°C) during the 1981–2005 period, averaged across longitude 21°–34° E and latitude 17.4°–7.6° S

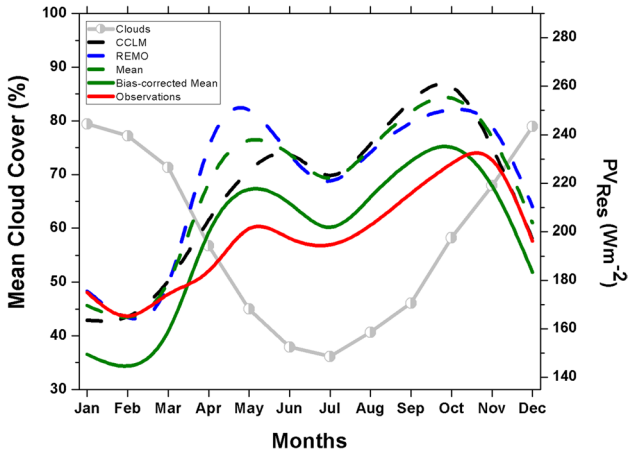

Fig. 7 Mean annual cycle of cloud cover (%), observed and modeled photovoltaic solar power resource (PV_{Res}; W/m^2) during the 1981–2005 period, averaged across longitude 21°–34° E and latitude 17.4°–7.6° S

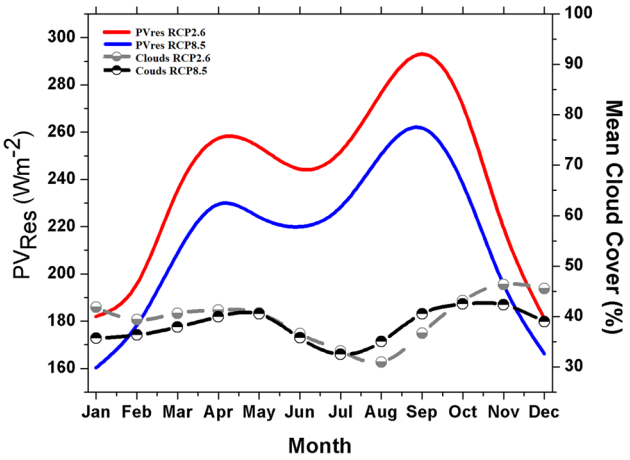

Fig. 8 Projections of the annual cycle of photovoltaic solar power resource (PV_{Res}; W/m^2) for the period 2025–2100 and mean annual cycle of cloud cover for low, medium, and high clouds (%), averaged across longitude 21°–34° E and latitude 17.4°–7.6° S

3.2 Future evolution of solar photovoltaic energy resources (PV_{Res})

3.2.1 Future temporal evolution of PV_{Res}

For the future, results indicate that at an average of 237 W/m^2 and 212 W/m^2, respectively, RCP2.6 leads to 12 ± 3% more PV_{Res} than RCP8.5 (Fig. 8). However, an exploration of the future seasonal cycle of mean cloudiness does not show major differences between RCP2.6 and RCP8.5 (Fig. 8); therefore, the observed less PV_{Res} in RCP8.5 can be attributed to higher near-surface temperature, thus making PV less efficient. However, no major changes are expected with regard to the annual cycle. Under RCP2.6, January and February are still expected to be characterized by relatively low PV_{Res} values ranging between 149 and 235 W/m^2 while the highest PV_{Res} values of up to ~ 300 W/m^2 are expected in September. Similarly, under RCP8.5, the lowest PV_{Res} values

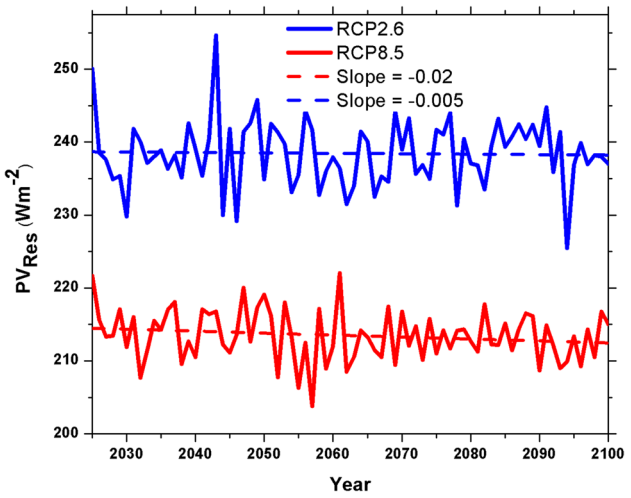

Fig. 9 Projections of the spatial mean of photovoltaic solar power resources (PV_{Res}; W/m^2) for the period 2025–2100 averaged across longitude 21°–34° E and latitude 17.4°–7.6° S

are expected in January and February ranging between 130 and 180 W/m^2.

These findings suggest that regardless of the emission scenario, seasonality will be the major factor affecting PV_{Res} in the future (Wiltberger et al. 2009). One key observation is that the January and February period when the country is expected to experience the lowest PV_{Res} coincides with the time the country is characterized by lower wind power densities which also peak around August coincidentally with PV_{Res} (Libanda and Paeth 2022). Thus, our findings embodied point toward a wind–solar energy mix for enhancing production during peak times, but a substitutionary energy source such as hydropower may be necessary during months of low production. The peak of wind speed around August is also advantageous to enhance PV_{Res} because wind cools solar panels, making them more efficient (Gökmen et al. 2016). It is important to note that solar panels generate electricity with sunlight and not heat. Atoms get energized to a higher level in the presence of sunlight, thus leading to electricity generation (Tisdale et al. 2010). However, atoms tend to vibrate faster in a hot solar cell than in a cooler one. Electrons in a solar panel whose temperature is cooled by 1 °C are 0.05% more efficient (Glenn 2019), thus the cooling effect of wind on PV_{Res} is beneficial.

The year-to-year variations indicate a very negligible but statistically significant decrease in PV_{Res} of 0.02 W/m^2 under RCP2.6 and 0.005 W/m^2 under RCP8.5 (Fig. 9). The highest PV_{Res} values are expected toward the middle of the century reaching their peak of ~ 316 W/m^2 under RCP2.6 between 1930 and 1960 and 281 W/m^2 between 1950 and 1970 under RCP8.5. Similar observations were made in the Sahel-Savannah region where progressive PV_{Res} decreases of up to 2% were found, becoming more pronounced and reaching a high of − 3.5% in the far future (Ndiaye et al. 2022). The decrease of PV_{Res} especially toward the end of the century can be explained by the expected temperature increments toward 2100. Although the projected PV_{Res} decrease will affect the size of future solar projects in Zambia, it is unlikely to have a significant effect on their viability (Bichet et al. 2019).

3.2.2 Future spatial evolution of PV_{Res}

Results of the future spatial trend of PV_{Res} indicate that although on average Zambia is expected to experience slight reductions (Fig. 10), there are spatial differences across the country with some places such as Eastern Province being expected to experience a negligible positive annual trend of up to 0.003 W/m^2 (Fig. 10). Both RCP2.6 and RCP8.5 agree on the trend of PV_{Res} across Eastern Province, they, however, disagree across Western Province where RCP2.6 projects a slight upward trend while RCP8.5 projects a downward trend (Fig. 10A, B, respectively). Given the marginal differences, what stands out from these results is that future changes of PV_{Res} in Zambia are likely to be near zero.

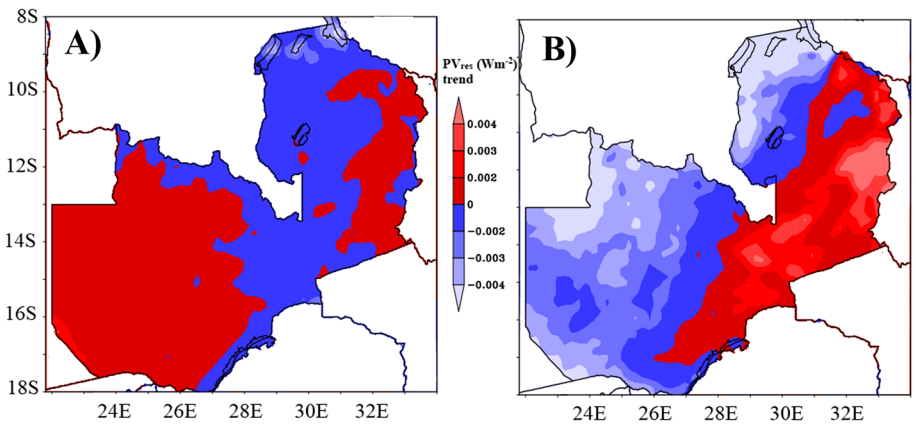

Fig. 10 Projections of the future spatial trend of PV_{Res} (W/m^2) across Zambia for **A** RCP2.6 and **B** RCP8.5 for the period 2025–2100

4 Concluding thoughts

We set out to explore future variations of climatic variables with a focus on changes in future photovoltaic power resources (PV_{Res}) over Zambia. We used CORDEX-CORE simulations over the Africa domain to study future PV_{Res} for the period 2025–2100. The main findings of this study can be summarized as follows:

- Regional Climate Models REMO, CCLM, and the mean reproduce wind speed, SR, and TAS better than RegCM.
- Temporally, RCMs were found to accurately reproduce the annual cycle of wind speed, SR, and TAS although overestimations are evident, thus necessitating bias corrections before analyzing future simulations.
- RCP2.6, a greener and climate-friendly pathway, points toward $12 \pm 3\%$ better renewable energy across Zambia compared to RCP8.5.
- Spatially, some positive trends are evident especially across Eastern Province although these are very marginal, thus suggesting that future changes of PV_{Res} in Zambia are likely to be near zero.

Given seasonal fluctuations of PV_{Res}, the present analysis showed that a wind-solar energy mix has a lot of promise for enhancing production during peak times, but a substitutionary energy source may be necessary during months of low production. While this study has highlighted key future spatiotemporal PV_{Res} trends in Zambia, it suffers from the lack of robust reliable observational datasets and a limited number of models. Furthermore, it is important to note that the multi-model ensemble used herein does not factor in the influence of aerosols on PV_{Res} projections. Aerosols are well known to be strong modulators of SR (Mallet et al. 2021) and clouds (Deroubaix et al. 2022), consequently PV_{Res} especially in arid environments (Neher et al. 2019). Nevertheless, although RegCM inherently has an aerosol module, its unrealistic simulation of the past climate of Zambia suggests that including it in the ensemble would lead to larger biases. It is also notable that types of aerosols included in RegCM (e.g., Sea salt and dust; Solmon et al. 2006; Zakey et al. 2006, 2008) are not common in Zambia. Future PV_{Res} investments in Zambia should, therefore, be undertaken after addressing these limitations thoroughly.

Acknowledgements This work was financially supported by the Alexander von Humboldt (AvH) Foundation, the foundation is hereby acknowledged. It should be noted, however, that the AvH Foundation was not involved in the conception, analytical design, data analyses, interpretation of the data, manuscript writing, or the decision to submit this work for publication. As such, this work cannot be construed as a reflection of the position of the AvH Foundation.

Funding Open Access funding enabled and organized by Projekt DEAL.

Data Availability Air temperature data (TAS) from Climatic Research Unit data is available at: https://crudata.uea.ac.uk/cru/data/hrg/. The fifth-generation global climate reanalysis (ERA5) data is available at: https://www.ecmwf.int/en/forecasts/dataset/ecmwf-reanalysis-v5. Solar radiation data is available at: https://www.climatologylab.org/terraclimate.html. CORDEX-CORE datasets are available at: https://cordex.org/experiment-guidelines/cordex-core/.

Declarations

Conflict of interest The authors declare no potential conflict of interest.

References

Abudu, H., Wesseh, P. K., and Lin, B. (2023). Are African countries on track to achieve their NDCs pledges? Evidence from difference-in-differences technique. Environmental Impact Assessment Review, 98, 106917. https://doi.org/10.1016/j.eiar.2022.106917

Adamowski K, Prokoph A, Adamowski J (2009) Development of a new method of wavelet aided trend detection and estimation. Hydrol Process 23(18):2686–2696. https://doi.org/10.1002/hyp.7260

Africa Groundwater Atlas. 2019. Climate. British Geological Survey. Available online at: https://www.bgs.ac.uk/geology-projects/africa-groundwater-atlas/ [Accessed 16 January 2023]

Agbo EP, Nkajoe U, Edet CO (2022) Comparison of Mann-Kendall and Şen's innovative trend method for climatic parameters over Nigeria's climatic zones. Clim Dyn. https://doi.org/10.1007/s00382-022-06521-9

Bartók B, Tobin I, Vautard R, Vrac M, Jin X, Levavasseur G, Denvil S, Dubus L, Parey S, Michelangeli PA, Troccoli A, Saint-Drenan YM (2019) A climate projection dataset tailored for the European energy sector. Clim Serv 16: 100138. https://doi.org/10.1016/j.cliser.2019.100138

Bichet A, Hingray B, Evin G, Diedhiou A, Kebe CMF, Anquetin S (2019) Potential impact of climate change on solar resource in Africa for photovoltaic energy: analyses from CORDEX-AFRICA climate experiments. Environ Res Lett 14(12): 124039. https://doi.org/10.1088/1748-9326/ab500a

Blal M, Khelifi S, Dabou R, Sahouane N, Slimani A, Rouabhia A, Ziane A, Neçaibia A, Bouraiou A, Tidjar B (2020) A prediction models for estimating global solar radiation and evaluation meteorological effect on solar radiation potential under several weather conditions at the surface of Adrar environment. Measurement 152: 107348. https://doi.org/10.1016/j.measurement.2019.107348

Cattiaux J, Douville H, Peings Y (2013) European temperatures in CMIP5: origins of present-day biases and future uncertainties. Clim Dym 41(11–12):2889–2907

Chenni R, Makhlouf M, Kerbache T, Bouzid A (2007) A detailed modeling method for photovoltaic cells. Energy 2007(32):1724–1730

Colfescu I, Cowan T, Doblas-Reyes F, Eden J, Hauser M, Hegerl G, Hempelmann N, Klehmet K, Lott F, Nangini C, Orth R, Radanovics S, Seneviratne SI, van Oldenborgh GJ et al (2019) Evaluation of the HadGEM3-A simulations in view of detection and attribution of human influence on extreme events in Europe. Clim Dyn 52(1–2):1187–1210

Costoya X, deCastro M, Carvalho D, Feng Z, Gómez-Gesteira M (2021) Climate change impacts on the future offshore wind energy resource in China. Renewable Energy 175:731–747. https://doi.org/10.1016/j.renene.2021.05.001

Costoya X, deCastro M, Carvalho D, Arguilé-Pérez B, Gómez-Gesteira M (2022) Combining offshore wind and solar photovoltaic energy to stabilize energy supply under climate change scenarios: A case study on the western Iberian Peninsula. Renew Sustain Energy Rev 157: 112037. https://doi.org/10.1016/j.rser.2021.112037

Diesendorf M, Elliston B (2018) The feasibility of 100% renewable electricity systems: A response to critics. Renew Sustain Energy Rev 93:318–330. https://doi.org/10.1016/j.rser.2018.05.042

Doms G, Forstner J, Heise E, Herzog H-J, Raschendorfer M, Schrodin R, Reinhardt T, Vogel G (2007) A Description of the Nonhydrostatic Regional Model LM, Part II: Physical Parameterization; Deutscher Wetterdienst: Offenbach, Germany.

ECMWF (2022) Copernicus Climate Change Service – Global Impacts. Available at: https://climate.copernicus.eu/sites/default/files/2021-01/infosheet7.pdf [Accessed: 18 June 2023]

EU (2022) Renewable energy targets. Available online: https://energy.ec.europa.eu/topics/renewable-energy/renewable-energy-directive-targets-and-rules/renewable-energy-targets_en [Accessed: 30/12/2022]

Ebita A, Kobayashi S, Ota Y, Moriya M, Kumabe R, Onogi K, Harada Y, Yasui S, Miyaoka K, Takahashi K, Kamahori H, Kobayashi C, Endo H, Soma M, Oikawa Y, Ishimizu T (2011) The Japanese 55-year Reanalysis "JRA-55": An Interim Report. SOLA 7:149–152. https://doi.org/10.2151/sola.2011-038

Fick SE, Hijmans RJ (2017) WorldClim 2: new 1-km spatial resolution climate surfaces for global land areas. Int J Climatol 37(12):4302–4315. https://doi.org/10.1002/joc.5086

Foster and Elzing, United NationWebsite, December 2015. Available online: https://www.un.org/en/chronicle/article/role-fossil-fuels-sustainable-energy-system [accessed on 2 November 2022].

Giorgi F, Coppola E, Jacob D, Teichmann C, Abba Omar S, Ashfaq M, Ban N, Bülow K, Bukovsky M, Buntemeyer L, Cavazos T, Ciarlo`, J., da Rocha, R. P., Das, S., di Sante, F., Evans, J. P., Gao, X., Giuliani, G., Glazer, R. H., … Weber, T. (2022) The CORDEX-CORE EXP-I Initiative: Description and Highlight Results from the Initial Analysis. Bull Am Meteor Soc 103(2):E293–E310. https://doi.org/10.1175/bams-d-21-0119.1

Giorgi, F., Coppola, E., Solmon, F., Mariotti, L., Sylla, M., Bi, X., Elguindi, N., Diro, G., Nair, V., Giuliani, G., Turuncoglu, U., Cozzini, S., Güttler, I., O'Brien, T., Tawfik, A., Shalaby, A., Zakey, A., Steiner, A., Stordal, F., . . . Brankovic, C. (2012). RegCM4: model description and preliminary tests over multiple CORDEX domains. Climate Research, 52, 7–29. https://doi.org/10.3354/cr01018

Glenn H (2019) How Do Wind and Humidity Affect Solar Panel Efficiency? Available at: https://www.solar.com/learn/how-do-wind-and-humidity-affect-solar-panel-efficiency/. [Accessed 01/02/2023]

Green Tumble (2022). How Hot Do Solar Panels Get? Effect of Temperature on PV Panel Efficiency. Available at: https://greentumble.com/effect-of-temperature-on-solar-panel-efficiency/ [Accessed: 27/01/2022]

Gutowski JW, Giorgi F, Timbal B, Frigon A, Jacob D, Kang HS, Raghavan K, Lee B, Lennard C, Nikulin G et al (2016) WCRP COordinated Regional Downscaling EXperiment (CORDEX): A diagnostic MIP for CMIP6. Geosci Model Dev 9:4087–4095

Gökmen N, Hu W, Hou P, Chen Z, Sera D, Spataru S (2016) Investigation of wind speed cooling effect on PV panels in windy locations. Renewable Energy 90:283–290. https://doi.org/10.1016/j.renene.2016.01.017

Hamed, K.H., Rao, A.R., 1998. A modified Mann-Kendall trend test for autocorrelated data. J. Hydrol. 204 (1–4), 182–196. https://doi:https://doi.org/10.1016/S0022-1694(97)00125-X.

Harris I, Osborn TJ, Jones P, Lister D (2020b) Version 4 of the CRU TS monthly high-resolution gridded multivariate climate dataset. Scientific Data, 7(1). https://doi.org/10.1038/s41597-020-0453-3

Hartley A, Turnock S (2021) What are the benefits of reducing global CO_2 emissions to net-zero by 2050? Weather 77(1):27–28. https://doi.org/10.1002/wea.4111

Hersbach, H., Bell, B., Berrisford, P., Hirahara, S., Horányi, A., Muñoz-Sabater, J., Nicolas, J., Peubey, C., Radu, R., Schepers, D., Simmons, A., Soci, C., Abdalla, S., Abellan, X., Balsamo, G., Bechtold, P., Biavati, G., Bidlot, J., Bonavita, M., . . . Thépaut, J. (2020). The ERA5 global reanalysis. Quarterly Journal of the Royal Meteorological Society, 146(730), 1999–2049. https://doi.org/10.1002/qj.3803

Herwartz, D., Pack, A., & Nagel, T. J. (2021). A CO_2 greenhouse efficiently warmed the early Earth and decreased seawater $^{18}O/^{16}O$ before the onset of plate tectonics. Proceedings of the National Academy of Sciences, 118(23). https://doi.org/10.1073/pnas.2023617118

Herzog, H.-J.; Schubert, U.; Vogel, G.; Fiedler, A.; Kirchner, R. (2002). LLM - The High-Resolving Nonhydrostatic Simulation Model in the DWD-Project LITFASS. Part I: Modelling Technique and Simulation Method; COSMO Technical Report No. 4; Deutscher Wetterdienst: Offenbach, Germany.

Holtslag AAM, De Bruijn EIF, Pan HL (1990) A high-resolution air mass transformation model for short-range weather forecasting. Mon Weather Rev 118:1561–1575

IEA (2019). Renewables 2019 - market analysis and forecast from 2019 to 2024. Available online: www.iea.org/renewables2019 (accessed on 4 March 2022).

IPCC (2014). Climate Change 2014: Synthesis Report. Contribution of Working Groups I, II and III to the Fifth Assessment Report of the Intergovernmental Panel on Climate Change [Core Writing Team, R.K. Pachauri and L.A. Meyer (eds.)]. IPCC, Geneva, Switzerland, 151 pp.

Ines AVM, Hansen JW (2006) Bias correction of daily GCM rainfall forcrop simulation studies. Agric for Meteorol 138:44–53. https://doi.org/10.1016/j.agrformet.2006.03.009

Irena. (2022). Renewable power generation costs in 2021. ISBN: 978–92–9260–452–3

Jacob D, Podzun R (1997) Sensitivity studies with the regional climate model REMO. Meteorog Atmos Phys 63(1):119–129. https://doi.org/10.1007/BF01025368

Jerez S, Tobin I, Vautard R, Mont´avez JP, L´opez-Romero JM, Thais F, Wild M. (2015) The impact of climate change on photovoltaic power generation in Europe. Nat Commun 6(1):1–8

Jones, P D, and Harris, I. (2013). CRU TS3.21: Climatic Research Unit (CRU) Time-Series (TS) Version 3.21 of High-resolution gridded data of month-by-month variation in climate (Jan. 1901–Dec. 2012). NCAS British Atmospheric Data Centre, 24th September 2013. doi:https://doi.org/10.5285/D0E1585D-3417-485F-87AE-4FCECF10A992

Kendall MG (1948) Rank correlation methods. Grifn, London. https://doi.org/10.2307/2333282

Kiehl JT, Hack JJ, Bonan GB, Boville BA, Briegleb BP, Williamson DL, Rasch PJ (1996) Description of the NCAR Community

Climate Model (CCM3); National Center for Atmospheric Research: Boulder. CO, USA
Lazard, (2020). Lazard's levelized cost of energy analysis — Version 14.0. Available at: https://www.lazard.com/media/451419/lazards-levelized-cost-of-energy-version-140.pdf. [Accessed: 08/11/2022]
Libanda B, Paeth H (2022) Modelling wind speed across Zambia: Implications for wind energy. Int J Climatol. https://doi.org/10.1002/joc.7826
Lohmann U, Roeckner E (1996) Design and performance of a new cloud microphysics scheme developed for the ECHAM general circulation model. Clim Dyn 12(8):557–572. https://doi.org/10.1007/bf00207939
Louis JF (1979) A parametric model of vertical eddy fluxes in the atmosphere. Bound-Layer Meteorol 17(2):187–202. https://doi.org/10.1007/bf00117978
Luderer G, Madeddu S, Merfort L, Ueckerdt F, Pehl M, Pietzcker R, Rottoli M, Schreyer F, Bauer N, Baumstark L, Bertram C, Dirnaichner A, Humpenöder F, Levesque A, Popp A, Rodrigues R, Strefler J, Kriegler E (2021) Impact of declining renewable energy costs on electrification in low-emission scenarios. Nat Energy 7(1):32–42. https://doi.org/10.1038/s41560-021-00937-z
Mallet M, Nabat P, Johnson BM, Michou M, Haywood J, Chen C, Dubovik O (2021) Climate models generally underrepresent the warming by Central Africa biomass-burning aerosols over the Southeast Atlantic. Sci Adv 7(41). https://doi.org/10.1126/sciadv.abg9998
Mann HB (1945) Nonparametric tests against trend. Econometrica. https://doi.org/10.2307/1907187
Marshall BD (2017) An assessment of climate change and stratification in Lake Kariba (Zambia-Zimbabwe). Lakes Reserv Res Manag 22(3):229–240. https://doi.org/10.1111/lre.12185
Mavromatakis F, Makrides G, Georghiou G, Pothrakis A, Franghiadakis Y, Drakakis E, Koudoumas E (2010) Modeling the photovoltaic potential of a site. Renew Energy 35:1387–1390
Meinshausen M, Smith SJ, Calvin K, Daniel JS, Kainuma MLT, Lamarque JF, Matsumoto K, Montzka SA, Raper SCB, Riahi K, Thomson A, Velders GJM, van Vuuren DP (2011) The RCP greenhouse gas concentrations and their extensions from 1765 to 2300. Clim Change 109(1–2):213–241. https://doi.org/10.1007/s10584-011-0156-z
Morcrette JJ, Smith L, Fourquart Y (1986) Pressure and temperature dependance of the absorption in longwave radiation parameterizations. Beitr Phys Atmos 59:455–469
Musonda B, Jing Y, Iyakaremye V, Ojara M (2020) Analysis of Long-Term Variations of Drought Characteristics Using Standardized Precipitation Index over Zambia. Atmosphere 11(12):1268. https://doi.org/10.3390/atmos11121268
NASA (2022). Climate change vital signs. Available online: https://go.nasa.gov/3hYcAlo. [Accessed: 30/12/2022]
Ndiaye A, Moussa MS, Dione C, Sawadogo W, Bliefernicht J, Dungall L, Kunstmann H (2022) Projected Changes in Solar PV and Wind Energy Potential over West Africa: An Analysis of CORDEX-CORE Simulations. Energies 15(24):9602. https://doi.org/10.3390/en15249602
Neher I, Buchmann T, Crewell S, Pospichal B, Meilinger S (2019) Impact of atmospheric aerosols on solar power. Meteorol Z 28(4):305–321. https://doi.org/10.1127/metz/2019/0969
Nkolola, M. (2021). 22 Years of Near-zero Cloud Cover Variability across Varying Geographical Landscapes of Southern Africa: A Surprising Anomaly. International Journal of Environment and Climate Change, 150–163. https://doi.org/10.9734/ijecc/2021/v11i730450
Nordeng, T.E. (1994) Extended Versions of the Convective Parametrization Scheme at ECMWF and Their Impact on the Mean and Transient Activity of the Model in the Tropics; Technical Report No. 206; European Centre for Medium-RangeWeather Forecasts: Reading, UK, available at: https://www.ecmwf.int/node/11393 [Accessed: 18/01/2023]
Ogunjobi K.O, Ajayi V.O, Folorunsho A.H & Ilori O.W. (2022). Projected changes in wind energy potential using CORDEX ensemble simulation over West Africa. Meteorology and Atmospheric Physics, 134(3). https://doi.org/10.1007/s00703-022-00880-y
Pal JS, Small EE, Eltahir EAB (2000) Simulation of regional-scale water and energy budgets: Representation of subgrid cloud and precipitation processes within RegCM. J Geophys Res Atmos 105:29579–29594
Patakamuri S, O'Brien N (2021). modifiedmk: Modified Versions of Mann Kendall and Spearman's Rho Trend Tests_. R package version 1.6, Available at: https://CRAN.R-project.org/package=modifiedmk. [Accessed 22/01/2023]
Peel MC, Finlayson BL, McMahon TA (2007) Updated world map of the Köppen-Geiger climate classification. Hydrology and Earth System Science 11:1633–1644. https://doi.org/10.5194/hess-11-1633-2007
Perkins SE, Pitman AJ, Holbrook NJ, McAneney J (2007) Evaluation of the AR4 Climate Models' Simulated Daily Maximum Temperature, Minimum Temperature, and Precipitation over Australia Using Probability Density Functions. J Clim 20(17):4356–4376. https://doi.org/10.1175/jcli4253.1
Pfeifer, A., Herc, L., Batas Bjelić, I., & Duić, N. (2021). Flexibility index and decreasing the costs in energy systems with high share of renewable energy. Energy Conversion and Management, 240, 114258. https://doi.org/10.1016/j.enconman.2021.114258
R Core Team. (2020) R: A Language and Environment for Statistical Computing. Vienna, Austria: R Foundation for Statistical Computing.
Radziemska E (2003) The effect of temperature on the power drop in crystalline silicon solar cells. Renew Energy 28(1):1–12
Ritter B, Geleyn JF (1992) A comprehensive radiation scheme for numerical weather prediction models with potential applications in climate simulations. Mon Weather Rev 120:303–325
Rockel B, Will A, Hense A (2008) The Regional Climate Model COSMO-CLM (CCLM). Meteorol Z 17(4):347–348. https://doi.org/10.1127/0941-2948/2008/0309
Shrestha M. (2015). Data analysis relied on Linear Scaling bias correction (V.1.0) Microsoft Excel file.
Solmon F, Giorgi F, Liousse C (2006) Aerosol modelling for regional climate studies: Application to anthropogenic particles and evaluation over a European/African domain. Tellus B Chem Phys Meteorol 58:51
Sonali P, Nagesh Kumar D (2013) Review of trend detection methods and their application to detect temperature changes in India. J Hydrol 476:212–227. https://doi.org/10.1016/j.jhydrol.2012.10.034
Spiridonov, V., Ćurić, M. (2021). Energy and Radiation. In: Fundamentals of Meteorology. Springer, Cham. https://doi.org/10.1007/978-3-030-52655-9_5
Steffen Kothe (2022). cmsaf: A Toolbox for CM SAF NetCDF Data. R package version 3.4.4. https://CRAN.R-project.org/package=cmsaf
Tesche M, Kumar M (2016) Solar Radiation over Four Cities of India: Trend analysis using Mann-Kendall Statistical Test. International Journal of Renewable Energy Research 6(4):1385–1395. https://doi.org/10.1234/ijrer.v6i4.4572
Tiedtke M (1989) A comprehensive mass flux scheme for cumulus parameterization in large-scale models. Mon Weather Rev 117:1779–1800
Tisdale WA, Williams KJ, Timp BA, Norris DJ, Aydil ES, Zhu XY (2010) Hot-Electron Transfer from Semiconductor Nanocrystals. Science 328(5985):1543–1547. https://doi.org/10.1126/science.1185509

Tonui J, Tripanagnostopoulos Y (2008) Performance improvement of PV/T solar collectors with natural air flow operation. Sol Energy 2008(82):1–12

Troccoli, A.; Goodess, C.; Jones, P.; Penny, L.; Dorling, S.; Harpham, C.; Dubus, L.; Parey, S.; Claudel, S.; Khong, D.-H.; et al. (2018). Creating a proof-of-concept climate service to assess future renewable energy mixes in Europe: An overview of the C3S ECEM project. Adv. Sci. Res. 15, 191–205.https://doi.org/10.3390/en15249602

UCSB (2020). Does temperature affect the amount of energy a solar panel receives? Available at: https://bit.ly/3WPCzKo [Accessed: 27/01/2022]

UN, (2015). Transforming our world : the 2030 Agenda for Sustainable Development, 21 October 2015, A/RES/70/1, available at: https://www.refworld.org/docid/57b6e3e44.html [accessed 8 November 2022]

USAID (2015) Greenhouse Gas Emissions in Zambia. Available at: https://shorturl.at/cnRW5 [Accessed: 18 June 2023]

Vautard, R., Christidis, N., Ciavarella, A., Alvarez-Castro, C., Bellprat, O., Christiansen, B.,

Wilcke RAI, Mendlik T, Gobiet A (2013) Multi-variable error correction of regional climate models. Clim Change 120:871–887. https://doi.org/10.1007/s10584-013-0845-x

Wiltberger, M., Weigel, R. S., Lotko, W., & Fedder, J. A. (2009). Modeling seasonal variations of auroral particle precipitation in a global-scale magnetosphere-ionosphere simulation. Journal of Geophysical Research: Space Physics, 114(A1), n/a-n/a. https://doi.org/10.1029/2008ja013108

Zakey AS, Solmon F, Giorgi F (2006) Implementation and testing of a desert dust module in a regional climate model. Atmos Meas Tech 6:4687–4704

Zakey, A.S.; Giorgi, F.; Bi, X. (2008). Modeling of sea salt in a regional climate model: Fluxes and radiative forcing. J. Geophys. Res. Earth Surf. 113.